AGU PUBLICATIONS

JGR

Journal of Geophysical Research: Solid Earth

RESEARCH ARTICLE
10.1002/2016JB013662

Special Section:
Rock Physics of the Upper Crust

Remagnetization of the Paleogene Tibetan Himalayan carbonate rocks in the Gamba area: Implications for reconstructing the lower plate in the India-Asia collision

Wentao Huang[1,2,3], Peter C. Lippert[3], Michael J. Jackson[4], Mark J. Dekkers[5], Yang Zhang[1], Juan Li[6], Zhaojie Guo[1], Paul Kapp[2], and Douwe J. J. van Hinsbergen[5]

[1]Key Laboratory of Orogenic Belts and Crustal Evolution, Ministry of Education, School of Earth and Space Sciences, Peking University, Beijing, China, [2]Department of Geosciences, University of Arizona, Tucson, Arizona, USA, [3]Department of Geology and Geophysics, University of Utah, Salt Lake City, Utah, USA, [4]Institute for Rock Magnetism, Department of Earth Sciences, University of Minnesota, Minneapolis, Minnesota, USA, [5]Department of Earth Sciences, Utrecht University, Utrecht, Netherlands, [6]State Key Laboratory of Mineral Deposit Research, School of Earth Sciences and Engineering, Nanjing University, Nanjing, China

Abstract The characteristic remanent magnetization (ChRM) isolated from Paleogene carbonate rocks of the Zongpu Formation in Gamba (28.3°N, 88.5°E) of southern Tibet has previously been interpreted to be primary. These data are pertinent for estimating the width of Greater India and dating the initiation of India-Asia collision. We have reanalyzed the published ChRM directions and completed thorough rock magnetic tests and petrographic observations on specimens collected throughout the previously investigated sections. Negative nonparametric fold tests demonstrate that the ChRM has a synfolding or postfolding origin. Rock magnetic analyses reveal that the dominant magnetic carrier is magnetite. "Wasp-waisted" hysteresis loops, suppressed Verwey transitions, high frequency-dependent in-phase magnetic susceptibility, and evidence that >70% of the ferrimagnetic material is superparamagnetic at room temperature are consistent with the rock-magnetic fingerprint of remagnetized carbonate rocks. Scanning electron microscopy observations and energy-dispersive X-ray spectrometry analysis confirm that magnetite grains are authigenic. In summary, the carbonate rocks of the Zongpu Formation in Gamba have been chemically remagnetized. Thus, the early Paleogene latitude of the Tibetan Himalaya and size of Greater India have yet to be determined and the initiation of collision cannot yet be precisely dated by paleomagnetism. If collision began at 59 ± 1 Ma at ~19°N, as suggested by sedimentary records and paleomagnetic data from the Lhasa terrane, then a huge Greater India, as large as ~3500–3800 km, is required in the early Paleogene. This size, in sharp contrast to the few hundred kilometers estimated for the Early Cretaceous, implies an ever greater need for extension within Greater India during the Cretaceous.

Key Points:
- Zongpu carbonate rocks in the Gamba area of southern Tibet are chemically remagnetized
- Remagnetization was induced by authigenic magnetite formed during oxidation of early diagenetic pyrite
- Collision at ~59 Ma requires a huge Greater India of ~3500–3800 km in early Paleogene, much larger than the width for the Early Cretaceous

Supporting Information:
- Supporting Information S1

Correspondence to:
W. Huang,
wentaohuang@email.arizona.edu

Citation:
Huang, W., P. C. Lippert, M. J. Jackson, M. J. Dekkers, Y. Zhang, J. Li, Z. Guo, P. Kapp, and D. J. J. van Hinsbergen (2017), Remagnetization of the Paleogene Tibetan Himalayan carbonate rocks in the Gamba area: Implications for reconstructing the lower plate in the India-Asia collision, *J. Geophys. Res. Solid Earth*, *122*, doi:10.1002/2016JB013662.

Received 19 OCT 2016
Accepted 31 JAN 2017
Accepted article online 2 FEB 2017

1. Introduction

Quantitative paleogeographic reconstruction of the India-Asia collision zone relies on high-quality paleomagnetic poles for both Asia- and India-derived rocks. Uncertainties in the timing, kinematics, and magnitude of crustal deformation in the Himalayas and Asia limit our ability to quantify the paleolatitude history of the southern margin of Asia (Lhasa terrane) and the northern margin of India (Tibetan Himalaya) from a global apparent polar wander path (GAPWaP) [*Torsvik et al.*, 2012] alone. Paleomagnetic data from Lhasa and the Himalaya are therefore required to better quantify the precollisional paleogeography. Paleomagnetic data from Lower Cretaceous strata of the Tibetan Himalaya show insignificant paleolatitudinal separation between the Tibetan Himalaya and the modern northern limit of the undeformed Indian continent (i.e., at the Main Frontal Thrust of the Himalaya) and thus indicate a small size of "Greater" India [*Klootwijk and Bingham*, 1980; *Huang et al.*, 2015c; *Yang et al.*, 2015; *Ma et al.*, 2016]. Paleomagnetic data from uppermost Cretaceous and Paleogene strata, however, show a paleolatitudinal separation of Tibetan Himalaya from India of some 2675 ± 700 km (N-S) or a very large Greater India [*Patzelt et al.*, 1996; *Dupont-Nivet et al.*, 2010; *Yi et al.*, 2011]. Taken together, these paleomagnetic observations suggest that the Tibetan Himalaya may have rifted and drifted away from India during the Cretaceous [*van Hinsbergen et al.*, 2012]. Paleomagnetic constraints on the initiation of the Tibetan Himalaya-Lhasa collision, defined as the time at

which the latitude of the Lhasa continental block of southernmost Asia overlaps with the latitude of the Tibetan Himalaya, yield collision ages not older than ~52–50 Ma [*Dupont-Nivet et al.*, 2010; *Najman et al.*, 2010; *Huang et al.*, 2013, 2015b; *Lippert et al.*, 2014; *Hu et al.*, 2016]. Geologic records, however, show that Asian-derived detritus was first deposited in Tibetan Himalaya strata as early as 59 ± 1 Ma [*DeCelles et al.*, 2014; *Hu et al.*, 2015, 2016], during which a time interval about 1000–1600 km of India-Asia convergence occurred. Current paleomagnetic and stratigraphic constraints are thus incompatible, and the discrepancy invites a critical reappraisal of the reliability of both data sets. An accurate and precise collision age is required to calculate the magnitude of postcollisional convergence between the two continents, which, in turn, is the starting point for understanding how and where strain is partitioned into the lithospheric shortening and subduction at convergent margins.

Paleomagnetic data acquired from Lower Cretaceous lavas and volcaniclastic sandstones of the Tibetan Himalaya have averaged geomagnetic paleosecular variation, show no evidence for inclination shallowing, cannot be explained by even a hypothetical remagnetization, are reproducible, and are therefore considered reliable and robust [*Klootwijk and Bingham*, 1980; *Huang et al.*, 2015c; *Yang et al.*, 2015; *Ma et al.*, 2016]. Latest Cretaceous and Paleogene paleomagnetic poles have been determined from carbonate rocks of the Zongshan Formation (71–65 Ma) and Zongpu Formation (62–52 Ma) exposed in the Gamba area of southern Tibet (Figure 1) [*Patzelt et al.*, 1996; *Yi et al.*, 2011; *Li et al.*, 2015]. Unlike detrital rocks, which can be strongly affected by inclination shallowing, carbonate rocks are less prone to compaction and are considered immune from inclination shallowing. They are, however, notorious for experiencing widespread remagnetization induced by enhanced temperature, chemical alteration, or secondary mineral growth [e.g., *Appel et al.*, 2012; *Dekkers*, 2012; *Elmore et al.*, 2012; *Jackson and Swanson-Hysell*, 2012]. For instance, pervasive remagnetization has been demonstrated for Jurassic and Paleogene carbonate rocks of the Tibetan Himalaya exposed in the Tingri area (~190 km west of Gamba; Figure 1a) [e.g., *Besse et al.*, 1984; *Liebke et al.*, 2013; *Huang et al.*, 2015c]. We therefore use an extensive suite of rock magnetic and petrographic tools for fingerprinting remagnetization to critically reassess the reliability of the interpreted characteristic remanent magnetization (ChRM) directions of the Paleogene Zongpu carbonate rocks in the Gamba area. We reanalyze the reported paleomagnetic data by applying nonparametric fold tests and comparing the bedding attitudes, ChRM directions and polarities, and lithologies of the four carbonate members of the Zongpu Formation. We then apply high-temperature thermomagnetic experiments; room temperature hysteresis measurements; and low-temperature hysteresis, susceptibility, and remanence tests. Finally, we use energy-dispersive X-ray spectrometry (EDS) and scanning electron microscopy (SEM) to chemically and visually characterize the magnetic minerals and their morphology. With this information, we reevaluate whether or not the ChRMs isolated from the Zongpu carbonate rocks are primary. We describe a mechanism for the remanence acquisition and its timing, and we also discuss the implications of our findings for quantifying the size of Greater India, as well as the timing of initiation of the India-Asia collision.

2. Geologic Background and Sampling

The Paleogene Tibetan Himalayan sedimentary successions were deposited onto the northern passive continental margin of the Indian plate (Figure 1a). They are particularly well exposed and studied near Gamba County, where they are subdivided from bottom to top into the Jidula, Zongpu, Enba, and Zhaguo formations (Figure 1b) [e.g., *Li et al.*, 2015]. The Zongpu Formation (~350 m thick) conformably overlies the Indian plate-derived clastic rocks of the Jidula Formation and unconformably underlies the Asia-derived clastic rocks of the Enba Formation. It accumulated on a carbonate ramp and is biostratigraphically dated to late Danian to Ypresian [*Li et al.*, 2015, and references therein]. It is divided into four members (I–IV). Member I (~195 m thick) is composed of thin- to medium-bedded yellowish-grey limestones and marly limestones with green algae and foraminifera; Members II (~80 m thick) and III (~40 m thick) mainly consist of dark grey nodular limestone and nodular marls, respectively. Member IV (~25 m thick) includes grey massive and thick-bedded limestones and has a grey, thick-bedded conglomerate with limestone clasts at the base, indicating a sedimentary hiatus and disconformable contact between Members III and IV (Figures 1c and 1d) that corresponds with the Paleocene-Eocene boundary [*Li et al.*, 2015].

Previous paleomagnetic sampling of the Zongpu Formation was mainly located around Gamba County [*Patzelt et al.*, 1996; *Yi et al.*, 2011]. *Patzelt et al.* [1996] also reported paleomagnetic data from the Zongpu

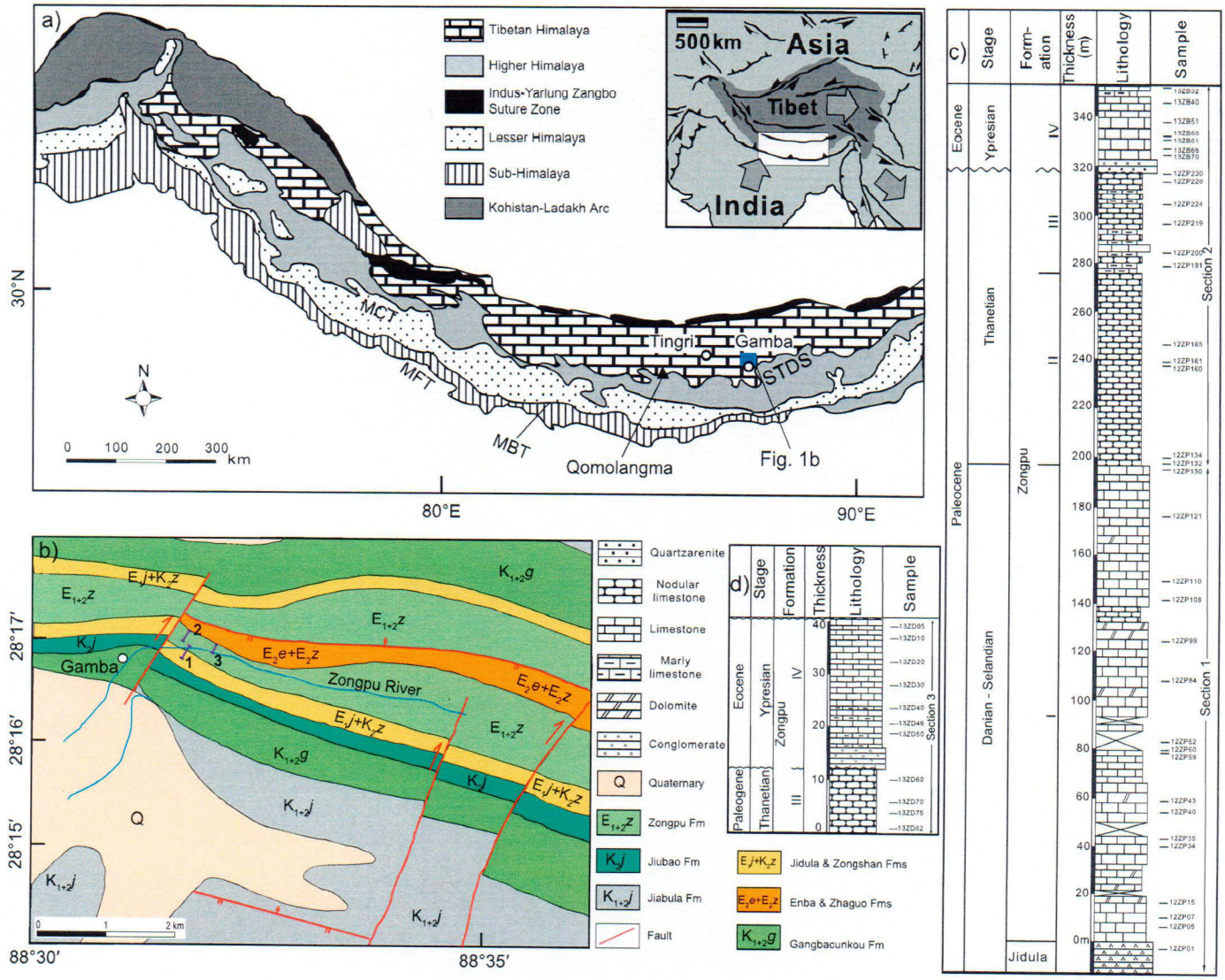

Figure 1. (a) Simplified geologic map of the Himalayas, modified from *Li et al.* [2015]. MFT: Main Frontal Thrust, MBT: Main Boundary Thrust, MCT: Main Central Thrust, STDS: Southern Tibetan Detachment System. (b) Geologic map of the Gamba area showing the studied stratigraphic sections, modified after *Li et al.* [2015]. (c and d) Lithostratigraphy of the Zongpu and uppermost Jidula Formations with the sampling localities indicated.

carbonate rocks near the Duina village (~75 km southeast of Gamba County). We collected 34 carbonate hand samples from the four members of the Zongpu Formation exposed in sections 1 and 2 (Figure 1c). Additionally, 11 samples from Members III and IV were also collected from section 3 to the east of sections 1 and 2 in Gamba (Figure 1d). One quartzarenite specimen (12ZP01) was also collected from the Jidula Formation below the Zongpu carbonate rocks in section 1. These sections overlap with the main sampling section A of the Zongpu Formation presented in *Yi et al.* [2011].

3. Reanalysis of the Paleomagnetic Results From the Zongpu Carbonate Rocks

In addition to their main sampling at section A of the Zongpu carbonate rocks, *Yi et al.* [2011] also collected samples from their section C near Tukson (~15 km southeast of Gamba County). Section C also contains Member I of the Zongpu Formation, but it has a different structural orientation from section A, making it possible to apply a regional fold test to constrain the timing of the remanence acquisition. *Yi et al.* [2011] reported a positive fold test, which has been used to argue that the Zongpu carbonate rocks at Gamba

carry primary remanence. The variation in bedding attitude within Member I and Members II–IV, however, also provides the opportunity to assess the origin of the ChRMs by performing an incremental fold test. We performed the nonparametric fold test of *Tauxe and Watson* [1994] on directions from Member I and found that optimal data clustering is reached at −16% to 47% untilting (Figure 2a). That is, the fold test is negative. A nonparametric fold test of ChRM directions from Members II to IV is also negative (Figure 2b). Moreover, we evaluated the ChRM directions from Members I to IV combined. Before tilt correction, the ChRM directions of Member I and Members II–IV have a common true mean direction (CTMD) with a classification of "A" (Figures 2a and 2b) [*McFadden and Lowes*, 1981; *McFadden and McElhinny*, 1990]. After tilt correction, however, the directions from Member I and Members II–IV show increased dispersion with the precision parameter k decreasing from 27.6 (in situ) to 22.7 (tilt corrected) (Figure 2c). The nonparametric fold test is clearly negative, with best grouping reached at 9% to 41% untilting (Figure 2c). In contrast to the positive fold test yielded from sections A and C, the fold tests applied to directions from just section A consistently yield negative results, implying that the ChRMs of the Zongpu carbonate rocks were acquired before the regional folding between sections A and C, but after the local folding of section A.

These field tests suggest that the ChRM directions observed in the Zongpu carbonate rocks in the Gamba area do not provide a faithful record of the geomagnetic field at the time of deposition. The magnetizations may instead have been acquired during multiphase folding of the Tibetan Himalaya strata, i.e., after initiation of the collision with Asia. Other lines of evidence previously used to argue for a primary origin of the remanence, including positive reversal tests, successful correlation to the geomagnetic polarity timescale (GPTS), and the apparent increase of ChRM inclination upsection (Figure 2d), will be discussed below. First, we present the results from systematic rock magnetic analyses to determine the carrier(s) of the remanence and their grain size distribution. These rock magnetic properties can be used to test for fingerprint remagnetization of carbonate rocks independent of directional constraints.

4. Rock Magnetism

Rock magnetic analyses, including thermomagnetic experiments; room temperature hysteresis measurements; and low-temperature hysteresis, susceptibility, and remanence experiments, were conducted at the Institute for Rock Magnetism at the University of Minnesota and the Utah Paleomagnetic Center at the University of Utah.

4.1. Thermomagnetic Runs

High-temperature, low-field susceptibility experiments were performed on 13 specimens by using a KLY-2 KappaBridge AC susceptibility meter with an AC field of 300 A m^{-1} and a frequency of 920 Hz. Specimens were heated in air from room temperature up to 650°C, and then cooled down to room temperature. All specimens, except 12ZP05 and 13ZD46, are characterized by a slow decrease of susceptibility before 400°C followed by a large increase in susceptibility before 500°C (Figure 3). This behavior is consistent with the formation of new magnetite by oxidation of pyrite [*Zegers et al.*, 2003]. All of the specimens show a sharp decrease in magnetization with increasing temperature up to 580°C (Figure 3). The Curie temperatures were determined to be 560–580°C from the first derivative of the measured data; these temperatures are typical for magnetite [*Dunlop and Ödemir*, 1997]. Some specimens also show additional loss of susceptibility up to 650°C (Figures 3a–3c, 3e, and 3g), indicating the presence of hematite [*Dunlop and Ödemir*, 1997]. The cooling curves for most specimens show large increases in susceptibility (Figures 3b–3i); this is caused by thermal alteration of pyrite and possibly other Fe-bearing minerals to magnetite during heating. We interpret this magnetic behavior to indicate the presence of magnetite and hematite in these specimens.

4.2. Room-Temperature Hysteresis Measurements

Hysteresis loops and backfield curves for 32 specimens were measured at room temperature by using a MicroMag Princeton Measurements vibrating sample magnetometer (VSM, nominal sensitivity of 5×10^{-9} A m^2) to determine the saturation magnetization (M_s), the saturation remanent magnetization (M_r), coercivity force (B_c), and remanent coercivity (B_{cr}). Seven specimens were too weak to provide interpretable loop and backfield curves and were excluded from our data set (Table S1 in the supporting information). Hysteresis loops for the remaining 25 specimens are all "wasp-waisted" (Figures 4a–4l), indicating the presence of two or more magnetic components with contrasting coercivities [*Jackson*, 1990; *Roberts et al.*, 1995] or

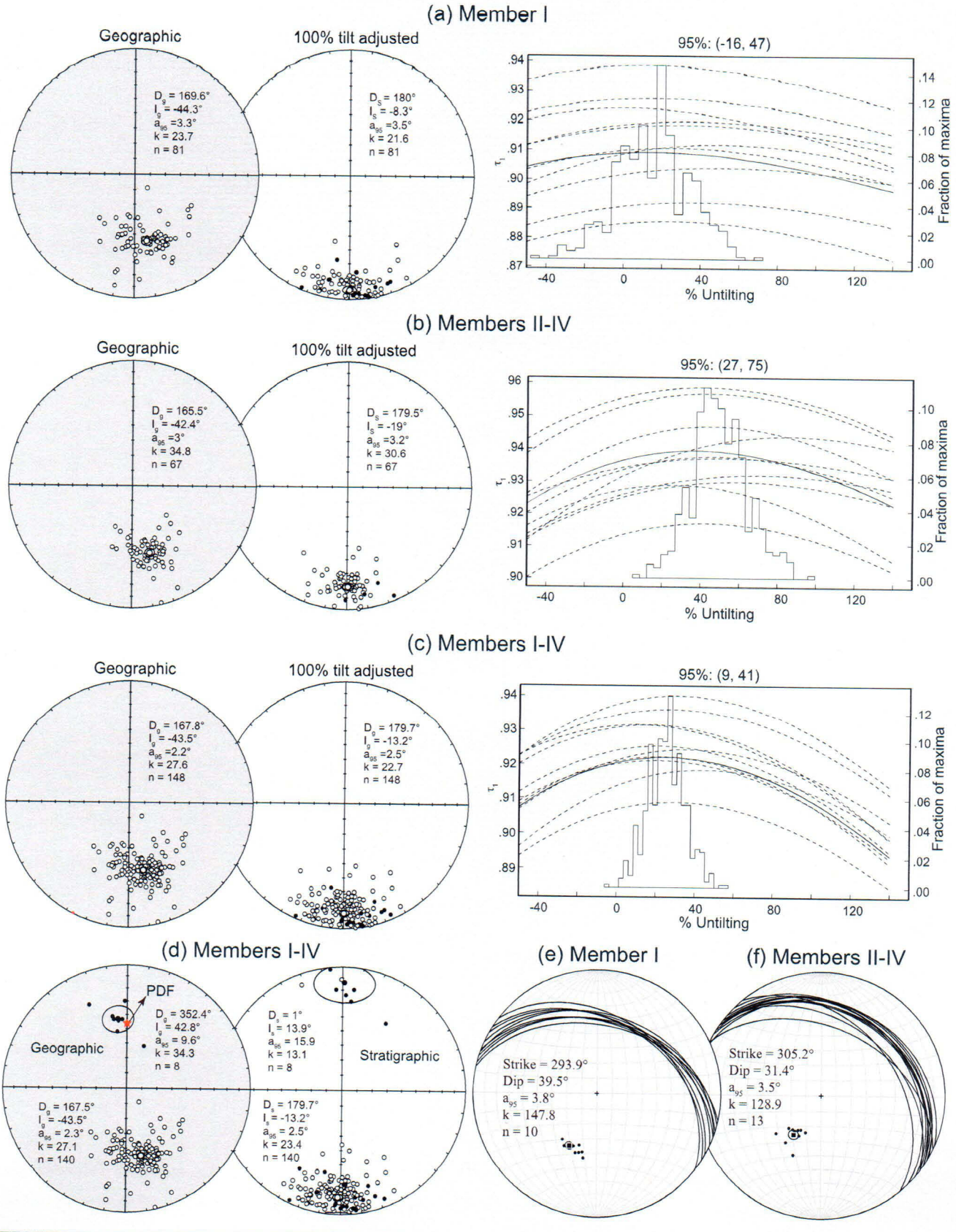
(a) Member I
Geographic
100% tilt adjusted
D_g = 169.6°
I_g = -44.3°
a_{95} =3.3°
k = 23.7
n = 81
D_S = 180°
I_S = -8.3°
a_{95} =3.5°
k = 21.6
n = 81
95%: (-16, 47)
τ_1
Fraction of maxima
% Untilting
(b) Members II-IV
Geographic
100% tilt adjusted
D_g = 165.5°
I_g = -42.4°
a_{95} =3°
k = 34.8
n = 67
D_S = 179.5°
I_S = -19°
a_{95} =3.2°
k = 30.6
n = 67
95%: (27, 75)
τ_1
Fraction of maxima
% Untilting
(c) Members I-IV
Geographic
100% tilt adjusted
D_g = 167.8°
I_g = -43.5°
a_{95} =2.2°
k = 27.6
n = 148
D_g = 179.7°
I_g = -13.2°
a_{95} =2.5°
k = 22.7
n = 148
95%: (9, 41)
τ_1
Fraction of maxima
% Untilting
(d) Members I-IV
PDF
Geographic
D_g = 352.4°
I_g = 42.8°
a_{95} = 9.6°
k = 34.3
n = 8
D_s = 1°
I_s = 13.9°
a_{95} = 15.9
k = 13.1
n = 8
Stratigraphic
D_g = 167.5°
I_g = -43.5°
a_{95} = 2.3°
k = 27.1
n = 140
D_s = 179.7°
I_s = -13.2°
a_{95} = 2.5°
k = 23.4
n = 140
(e) Member I
Strike = 293.9°
Dip = 39.5°
a_{95} = 3.8°
k = 147.8
n = 10
(f) Members II-IV
Strike = 305.2°
Dip = 31.4°
a_{95} = 3.5°
k = 128.9
n = 13

different size fractions of a single mineral [*Dunlop*, 2002]. The B_c and B_{cr} values for most specimens are low (Table S1), implying that the dominant magnetic carrier has a low coercivity. Most specimens are essentially saturated at 500 mT (Figures 4b–4e and 4j–4l); others show a slow approach to saturation and an irreversible magnetization in the field range of 0.5–1 T (Figures 4f–4i), indicating minor contribution from magnetic mineral(s) with high coercivity. A few specimens are far from saturation at 1 T (Figure 4a); the magnetic carriers of these specimens are probably a combination of ferrimagnetic and antiferromagnetic magnetic minerals, with low and high coercivities, respectively. These observations indicate that magnetite is the dominant contributor to the natural remanent magnetization (NRM) for most samples, and hematite, goethite, or both are minor contributors in some specimens. This is consistent with the results from the thermomagnetic experiments.

On a Day plot (Figure 4m), most hysteresis data plot near the superparamagnetic (SP) + single domain (SD) mixing curves [*Day et al.*, 1977; *Dunlop*, 2002]. The "wasp-waisted" shape of loops for a few specimens, such as 12ZP05 (Figure 4a), may be caused by a coexistence of low-coercivity magnetite and high-coercivity hematite, goethite, or both. However, the low B_c and B_{cr} values indicate that the "wasp-waisted" loops for most specimens cannot be attributed to hard antiferromagnetic admixtures (Table S1). Instead, they are likely the result of the combination of SD and fine-grained SP magnetite within the specimens.

4.3. Low-Temperature Hysteresis, Remanence, and Susceptibility Experiments

Although a population of SP grains has no contribution to NRM, it is important for understanding the origin of the (presumably) cogenetic stable single domain (SSD) grain population if the SSD grains are the large grain-size end member of the secondary magnetite. The SSD part is obviously a carrier of a geologically stable NRM. Magnetic properties of magnetite change dramatically with variation in grain size and temperature [*Néel*, 1949; *Dunlop and Ödemir*, 1997]. To further characterize the properties of the SP and SSD magnetite, we applied the following low-temperature experiments.

Low-temperature hysteresis measurements were also conducted on the VSM. The hysteresis loops of two specimens (13ZB32 and 13ZD20) were measured at 20 K–300 K with a temperature interval of 10 K. Although the signal/noise ratio is far from ideal, some significant features can be resolved. With the decrease of temperatures from 300 K to 20 K, both specimens show large and progressive increases in M_r and B_c. The shape of the loops also transforms from "wasp-waisted" to "pot-bellied" (Figures 5a–5c and 5g–5i), indicating that the SP fraction becomes thermally stable SSD with decreasing temperature. Quantitative loop analysis shows that M_s at 20 K is approximately two times greater than the room temperature value for 13ZB32 but only 0.4 times greater for 13ZD46 (Figures 5d and 5j and Tables S2 and S3). In 13ZB32 there appears to be an additional phase that magnetically orders at approximately 50 K; most of the increase in M_s is because of that. The increase in M_s from 300 K to 50 K is comparable to that for 13ZD46. The M_r values increase much more significantly over that same temperature interval: roughly 200% for 13ZB32 and 400% for 13ZD46 (Figures 5e and 5k and Tables S2 and S3). B_c and B_{cr} values are noisy, but they define an increasing trend with decreasing temperature (Tables S2 and S3). The shape parameter σ defined by *Fabian* [2003] quantifies the gradual change of the loops from strongly wasp-waisted ($\sigma > 0$ at room temperature) to pot-bellied ($\sigma < 0$ at low temperature) (Figures 5f and 5l). This transition occurs below 30 K for both specimens (Tables S2 and S3).

Low-temperature alternating current (AC) susceptibility experiments were run on a Quantum Design Magnetic Properties Measurement System (MPMS-5S). One specimen (12ZP59) was cooled in zero field to 20 K and then measured at several frequencies (1, 5.6, 31.6, 177.9, and 997.3 Hz) up to 300 K (Figure 6). At

Figure 2. (a–c) Nonparametric fold tests [*Tauxe and Watson*, 1994] using the ChRM directions of the Zongpu Formation from *Yi et al.* [2011]. Fold tests were applied separately to (a) Member I, (b) Members II–IV, and (c) Members I–IV of the Zongpu Formation. ChRM directions with normal polarity were all transferred to antipodal reversed polarities. Equal-area plots of the individual ChRM directions are displayed in (left) geographic coordinates and (middle) after 100% tilt correction. The decrease in k value indicates that the ChRM directions become more scattered after 100% tilt correction. (right) Bootstrapped statistics on the first eigenvalues (τ_1) show that best grouping in all the three fold tests is not reached at 100% untilting but at much lower values of tilting. (d) Equal-area plots of the individual ChRM directions of the Zongpu Formation from *Yi et al.* [2011] in (left) geographic and (right) stratigraphic coordinates. Note that ChRM directions with normal polarity plot very close to the direction of the present-day geomagnetic field (PDF) at the sampling locality, suggesting that these ChRMs might be a recent overprint. (e and f) Plot of the bedding attitude of Member I and Members II–IV strata of the Zongpu Formation. Note that the mean dip of Member I strata is ~8° steeper than that of Members II–IV strata.

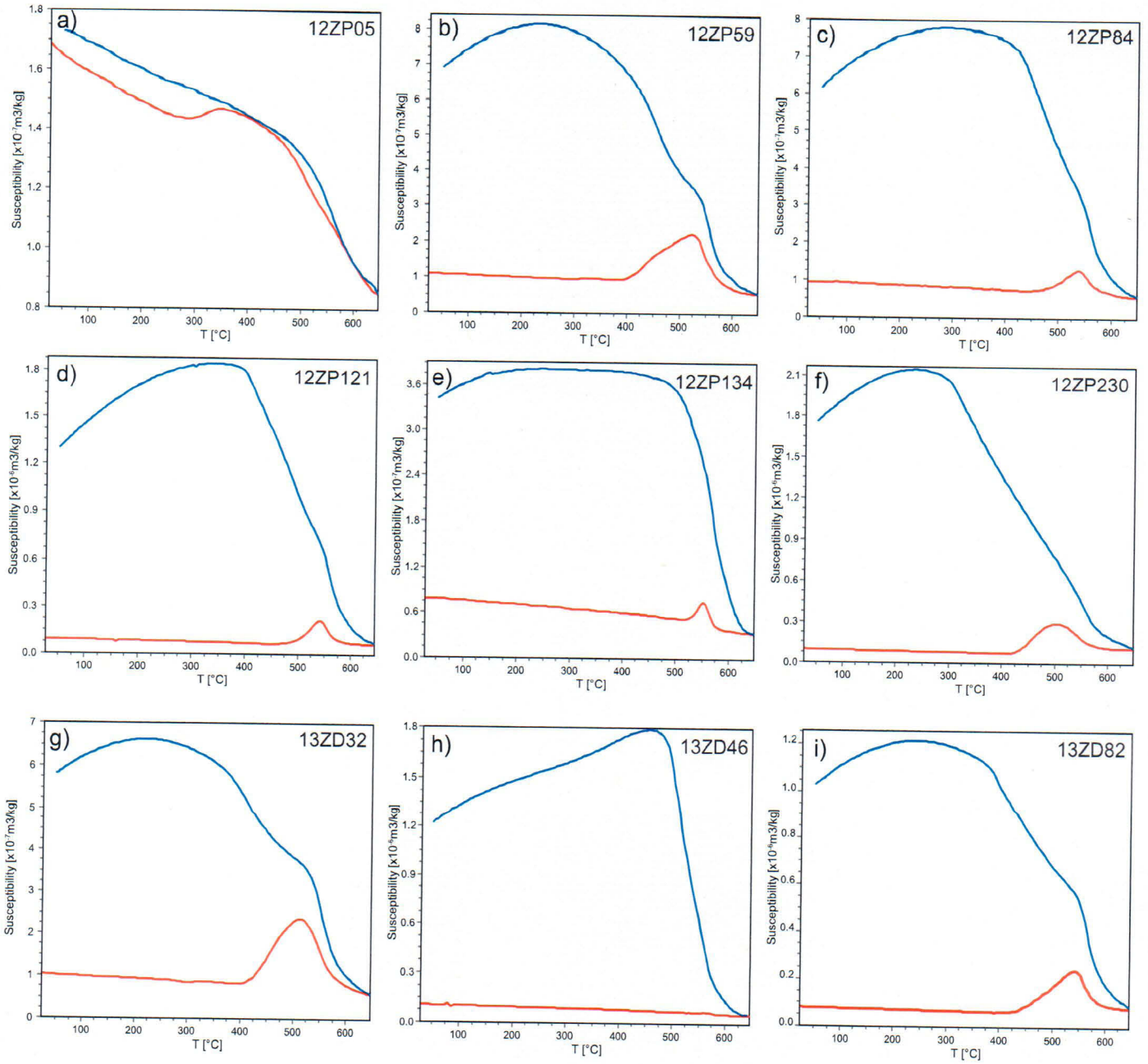

Figure 3. High-temperature heating (red) and cooling curves (blue) of bulk magnetic susceptibility in air for representative specimens.

room temperature, a relatively strong frequency dependence of susceptibility indicates the presence of a substantial population of grains with blocking temperatures near 300 K, which can be attributed to magnetite grains with diameters of 15–25 nm [*Worm and Jackson*, 1999; *Jackson and Swanson-Hysell*, 2012]. With decreasing temperature, the SP-SSD threshold shifts to smaller sizes and a strong frequency dependence of in-phase susceptibility (χ') can be observed down to 20 K (Figure 6a), indicating a broad distribution of nanosized magnetite. The measured out-of-phase susceptibility (χ'') is indistinguishable from the calculated values of $-(\pi/2)\, d\chi'/d(\ln(f))$, where f is the frequency, defined by the Néel relation (Figure 6b) [*Néel*, 1949], implying that χ'' originates primarily in a thermal relaxation mechanism.

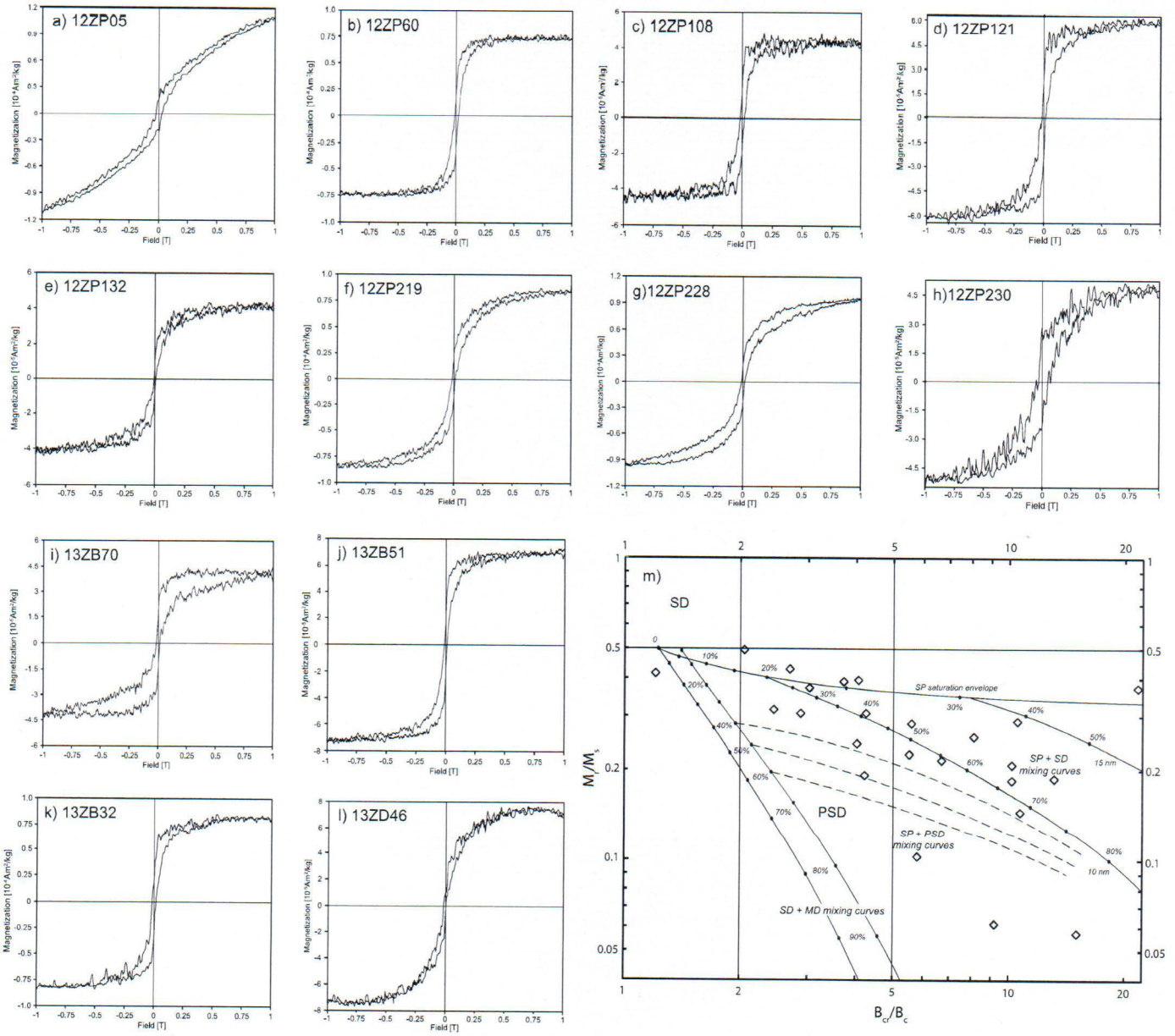

Figure 4. (a–l) Room temperature hysteresis loops from representative specimens of the Zongpu carbonate rocks. (m) Day plot [*Dunlop*, 2002] of the hysteresis parameters for Zongpu carbonate rocks.

Low-temperature remanence experiments were also run on the MPMS-5S. One specimen (12ZP230) underwent the field-cooled (FC) zero field-cooled (ZFC) low-temperature saturation isothermal remanent magnetization room temperature saturation isothermal remanent magnetization (RTSIRM) protocol, and 11 specimens underwent the more abbreviated sweep-cool-warm protocol. Low-temperature cooling of RTSIRM in all specimens shows a small change in magnetization associated with the Morin transition at approximately 225 K, indicating the minor presence of nanoparticle hematite [*Özdemir et al.*, 2008] (Figures 7a, 7b, 7d, and 7e). The broad maximum in cooling of RTSIRM around 50–150 K for some specimens (Figures 7a, 7b, and 7d) is probably caused by oxidized submicron magnetite [*Özdemir and Dunlop*, 2010]. The ZFC measurements show that more than 70% of remanence imposed isothermally by a 2.5 T field at 20 K is removed by warming to room temperature (Figures 7f–7j). Both RTSIRM and ZFC measurements for all of the specimens show no indication of the Verwey transition. The RT-SIRM cooling and warming cycles for

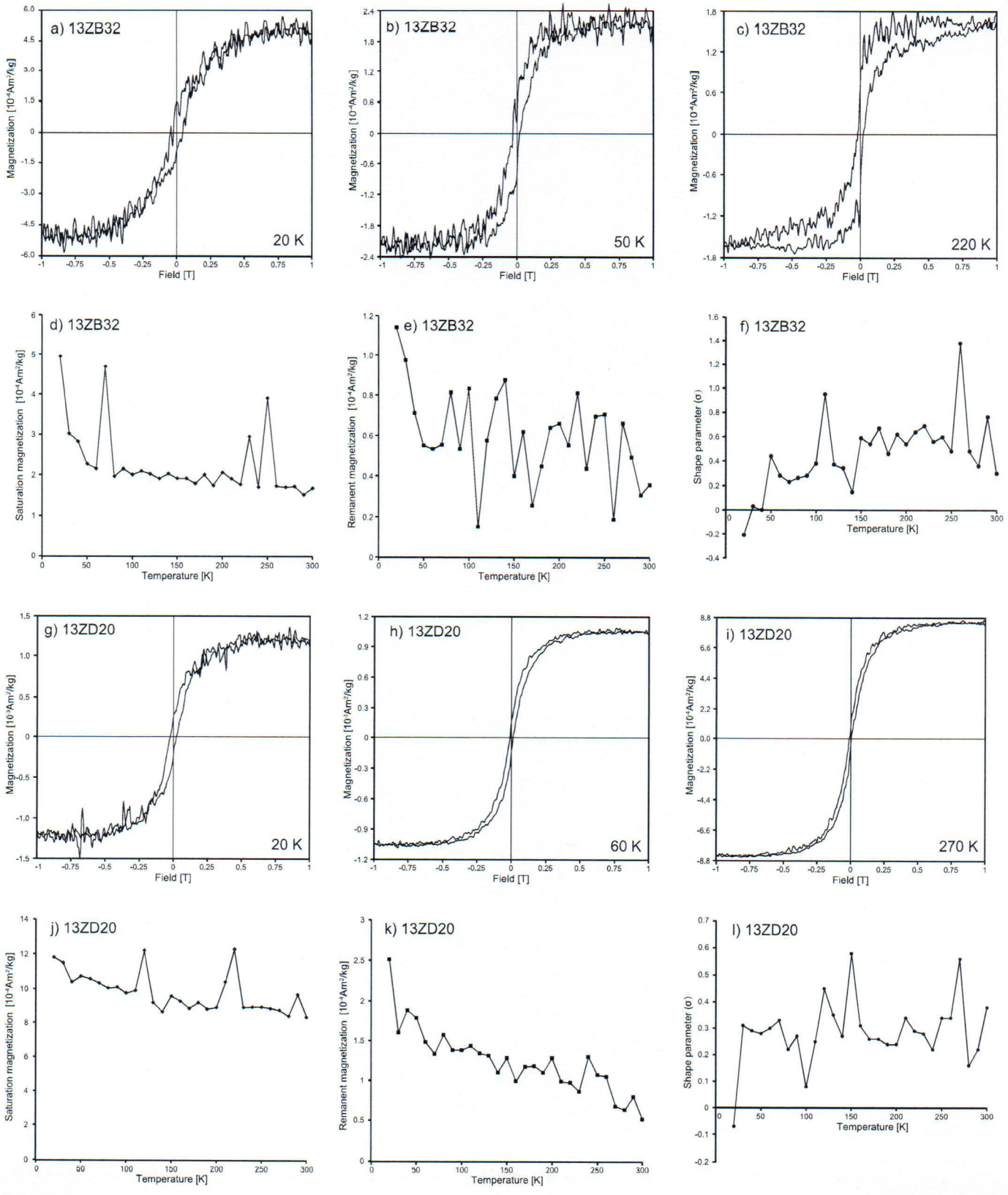
a) 13ZB32
20 K
Magnetization [10⁻⁴Am²/kg]
Field [T]
b) 13ZB32
50 K
Magnetization [10⁻⁴Am²/kg]
Field [T]
c) 13ZB32
220 K
Magnetization [10⁻⁴Am²/kg]
Field [T]
d) 13ZB32
Saturation magnetization [10⁻⁴Am²/kg]
Temperature [K]
e) 13ZB32
Remanent magnetization [10⁻⁴Am²/kg]
Temperature [K]
f) 13ZB32
Shape parameter (σ)
Temperature [K]
g) 13ZD20
20 K
Magnetization [10⁻³Am²/kg]
Field [T]
h) 13ZD20
60 K
Magnetization [10⁻³Am²/kg]
Field [T]
i) 13ZD20
270 K
Magnetization [10⁻³Am²/kg]
Field [T]
j) 13ZD20
Saturation magnetization [10⁻³Am²/kg]
Temperature [K]
k) 13ZD20
Remanent magnetization [10⁻³Am²/kg]
Temperature [K]
l) 13ZD20
Shape parameter (σ)
Temperature [K]

12ZP230 nearly overlap with each other (Figure 7c), whereas there is wide spread between ZFC and FC remanences, characteristic of goethite [e.g., *Guyodo et al.*, 2003]. Calculation of the particle size distribution from ZFC curves by using the method of *Worm and Jackson* [1999] indicates a broad, unimodal size distribution of the SP particles with peaks at or below 10^{-24} m^3 (10 nm in diameter) (Figures 7k–7o). This is in good agreement with plotting of most hysteresis data along the SP-SD mixing curves in the Day plot (Figure 4m) [*Dunlop*, 2002].

In summary, rock magnetic analyses reveal that nonstoichiometric nanoparticle magnetite is the dominant magnetic mineral in most specimens, whereas hematite has a minor contribution to the remanence in some specimens. There are also a few specimens with a nontrivial amount of hematite as the magnetic carrier. Magnetite has a broad grain size distribution, but most of it is in the SP range. SP magnetite cannot carry a stable, ancient magnetization, but its relative abundance strongly suggests that the stable SD magnetite fraction in these rocks was also formed authigenically.

5. SEM Observation and EDS Analysis

To identify the textural relationships and diagenetic conditions of magnetic minerals that may further help evaluate the origin of the remanence, polished thin sections of 20 representative specimens from the Zongpu carbonate rocks were investigated on a Field Electron and Ion GEG-650 scanning electron microscopy (SEM), operated at 12 or 15 kV and 40–60 nA at the SEM lab at the Key Laboratory of Orogenic Belts and Crustal Evolution, School of Earth and Space Sciences, Peking University (Beijing, China). EDS analysis was subsequently conducted to obtain compositional information. It is worth noting that only coarse-grained magnetite can be observed, whereas nanosized SP magnetite is far beyond the resolution of SEM.

SEM observations indicate three different morphologies of magnetic minerals in these specimens (Figure 8). We interpret each of these phases to be magnetite based on the EDS analysis (Figure S1 in the supporting information) and the rock magnetic results. Hematite was not observed in thin section. Iron sulfides with similar morphologies to magnetite but with brighter backscattered electron images are also detected (Figure 8). EDS analysis and thermomagnetic tests described in the previous section suggest that the iron sulfide is pyrite. One phase of magnetite is subeuhedral to euhedral with variable crystal sizes ranging from a few micrometers to 100 μm (Figures 8a, 8b, 8d, 8f–8i, 8q, 8r, and 8s). This population is the dominant form of magnetite in most specimens. A second phase is framboids aggregating up to 50 μm in diameter (Figures 8c, 8e, 8h, 8m, 8p, 8s, and 8t). The framboids occur in the calcite matrix (Figures 8e, 8o, 8s, and 8t) or in voids of the matrix (Figures 8c, 8h, 8m, and 8p). The third phase of magnetite coexists with pyrite in either a subeuhedral to euhedral (Figures 8j, 8k, 8n, and 8r) or framboidal morphology (Figures 8m and 8t). Pyrite with all these three phases of magnetite is also observed (Figures 8d, 8j–8n, and 8t). Morphologies of these magnetite grains are not consistent with a detrital or biogenetic origin [e.g., *Abrajevitch and Kodama*, 2009; *Chang et al.*, 2013]. Instead, it is more likely that some euhedral magnetite grains are late diagenetic minerals (Figure 8g), whereas others are pseudomorphs after euhedral or framboidal pyrite that oxidized during a later phase of diagenesis [e.g., *Suk et al.*, 1990]. The third phase of magnetite that coexists with pyrite probably indicates that the early diagenetic pyrite is partially oxidized, further supporting that most magnetite in the Zongpu carbonate rocks was formed by replacement of early diagenetic pyrite. In summary, SEM observation and EDS analysis suggest that the observed coarse-grained magnetite that carries the NRM in Zongpu carbonate rocks is authigenic.

6. Discussion

6.1. Does the Zongpu Formation in the Gamba Area Carry a Primary Remanence?

Compared to classic field tests, which provide only a relative constraint on the age of magnetization, rock magnetic characterization and petrographic observation are essential to evaluating the age and origin of the NRM [*Jackson and Swanson-Hysell*, 2012]. Remagnetization of carbonate rocks usually involves growth

Figure 5. Hysteresis loops for sample 13ZB32 at (a) 20 K, (b) 50 K, and (c) 220 K. The shape of the loops gradually changes from "pot-bellied" to "wasp-waisted" with increasing temperature. (d) Saturation remanence, (e) remanent magnetization, and (f) shape parameter of the loops as a function of temperature for sample 13ZB32. Hysteresis loops for sample 13ZD20 at (g) 20 K, (h) 60 K, and (i) 270 K. (j–l) Same as Figures 5d–5f but for sample 13ZD20.

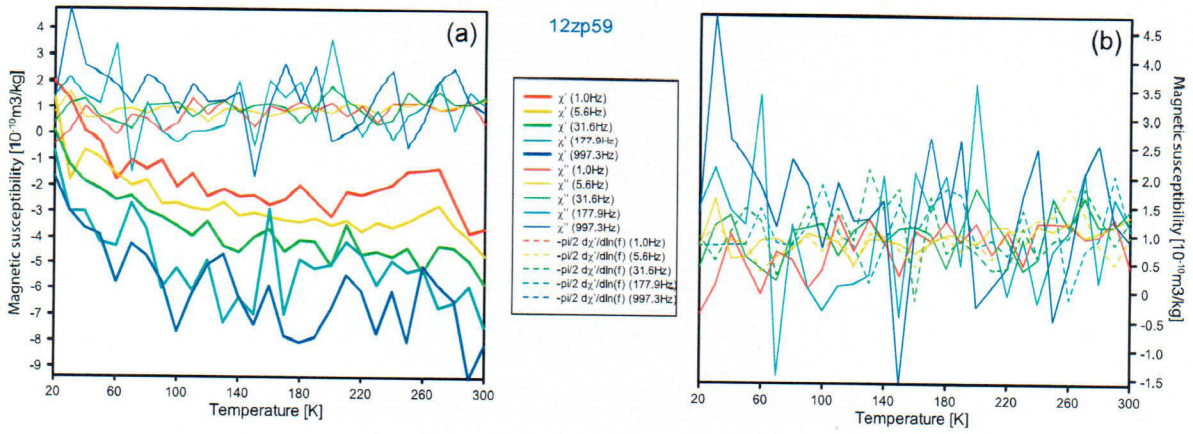

Figure 6. (a) In-phase and quadrature susceptibility at 1.0 Hz, 5.6 Hz, 31.6 Hz, 177.9 Hz, and 997.3 Hz for sample 12ZP59, measured from 20 to 300 K. Strong frequency dependence over the whole temperature range indicates a broad size distribution of nanoparticles. (b) Expanded view of quadrature susceptibilities compared to the derivative of in-phase susceptibility with respect to ln(*f*). Consistency between them implies that quadrature susceptibility originates primarily in a thermal relaxation mechanism.

of fine-grained magnetite, which is dominantly in the SP and SSD size range and has distinctive rock magnetic properties. These rock magnetic characteristics are commonly used as a "fingerprint" for diagnosing remagnetization. In the Day plot (Figure 4m), most specimens from the Zongpu carbonate rocks plot near the SP-SD mixing line, which overlaps with the plotted region of remagnetized limestones but differs from the SD + MD (multidomain) region of limestones carrying primary remanence [*Jackson and Swanson-Hysell*, 2012, and references therein]. The SP fraction of magnetite is further characterized by the low-temperature hysteresis, susceptibility, and remanence results, which show strong temperature dependence of the hysteresis parameters (Figure 5), strong frequency dependence of in-phase susceptibility (Figure 6a), and >70% of the ferromagnetic population smaller than the blocking volume of magnetite at room temperature (Figure 7). Although the SP fraction is not the carrier of the ancient NRM, we suggest that it has the same origin as the SSD magnetite. Unlike pelagic carbonate rocks, which may have significant contributions from detrital or biogenetic magnetite that carries the primary remanence [e.g., *Abrajevitch and Kodama*, 2009; *Chang et al.*, 2013], the Zongpu carbonate rocks accumulated on a carbonate ramp with low clastic influx and high carbonate saturation [*Li et al.*, 2015]. The low concentration of primary detrital magnetite is usually in pseudosingle domain MD size ranges, and these grains can be diminished in size to SP-SSD sizes by reductive dissolution during deposition and early diagenesis [e.g., *Smirnov and Tarduno*, 2001]. Given that marly limestones are common in the Zongpu Formation, it is also probable that the formation of the SP-SSD magnetite was related to clay diagenesis during which sorbed iron cations can be released and precipitate as magnetite [e.g., *Jackson et al.*, 1988]. Another potential authigenic mechanism involves the oxidization of early diagenetic pyrite to magnetite. We argue that extracellular formation [e.g., *Sparks et al.*, 1990] or aeolian delivery [e.g., *Lanci and Kent*, 2006] of SP magnetite is not a viable mechanism for the Zongpu carbonate rocks. These mechanisms for the origin of the SP-SSD magnetite, acting alone or in concert, can frequently change the magnetic mineralogy and NRM and result in remagnetization of a rock sequence. Our SEM observations and EDS analyses show no indication of primary detrital magnetite. Instead, we concluded that the observed subeuhedral-euhedral or framboidal magnetite grains are authigenic (Figure 8). Therefore, rock magnetic and petrographic investigations document and support the chemical remagnetization interpretation.

Previous paleomagnetic investigations of the Zongpu carbonate rocks in the Gamba area argued for a primary origin for the ChRM. This argument was based mainly on (1) positive fold tests, (2) positive reversal tests, (3) correlation of observed magnetic polarities to the GPTS, and (4) northward paleolatitudinal progress (inclination steepening) with decreasing rock age as expected from the northward drift of the Tibetan Himalaya in the early Paleogene [*Patzelt et al.*, 1996; *Yi et al.*, 2011]. Instead, our systematic reanalyses of the previously reported paleomagnetic results indicate a secondary origin for the remanence. So how can these contradicting interpretations be reconciled? To this end, we reevaluate the above arguments for a primary remanent magnetization. The positive fold test for the Zongpu carbonate rocks presented in *Patzelt et al.* [1996] was suggested by increased *k* values after tilt correction of a small data set. Our

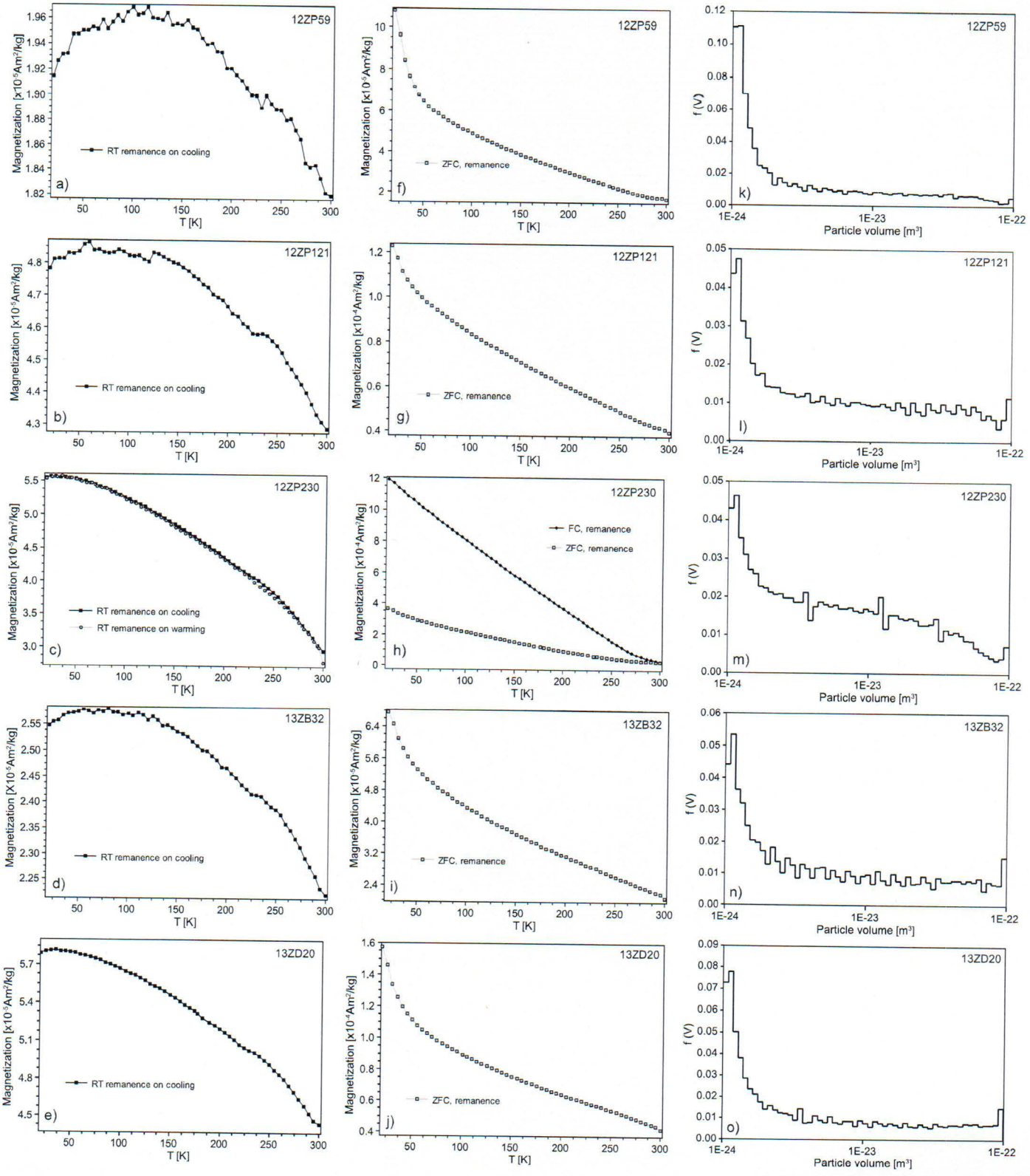
12ZP59
Magnetization [x10⁻⁵Am²/kg]
RT remanence on cooling
a)
T [K]
12ZP59
Magnetization [x10⁻⁵Am²/kg]
ZFC, remanence
f)
T [K]
12ZP59
f (V)
k)
Particle volume [m³]
12ZP121
Magnetization [x10⁻⁵Am²/kg]
RT remanence on cooling
b)
T [K]
12ZP121
Magnetization [x10⁻⁴Am²/kg]
ZFC, remanence
g)
T [K]
12ZP121
f (V)
l)
Particle volume [m³]
12ZP230
Magnetization [x10⁻⁵Am²/kg]
RT remanence on cooling
RT remanence on warming
c)
T [K]
12ZP230
Magnetization [x10⁻⁴Am²/kg]
FC, remanence
ZFC, remanence
h)
T [K]
12ZP230
f (V)
m)
Particle volume [m³]
13ZB32
Magnetization [X10⁻⁵Am²/kg]
RT remanence on cooling
d)
T [K]
13ZB32
Magnetization [x10⁻⁵Am²/kg]
ZFC, remanence
i)
T [K]
13ZB32
f (V)
n)
Particle volume [m³]
13ZD20
Magnetization [x10⁻⁵Am²/kg]
RT remanence on cooling
e)
T [K]
13ZD20
Magnetization [x10⁻⁴Am²/kg]
ZFC, remanence
j)
T [K]
13ZD20
f (V)
o)
Particle volume [m³]

reanalyses of a large number of ChRM directions reported by *Yi et al.* [2011] instead show that the *k* values for both Member I and Members II–IV decrease after tilt correction (Figures 2a and 2b). The positive fold test from *Yi et al.* [2011] relies on the results from a comparable section in the Tukson area (~15 km southeast of the Gamba County). This fold test is reliable but can only provide a loose constraint on acquisition time of the interpreted ChRM directions because secondary remanence may well have been acquired before this phase of folding. Our negative fold test results (Figures 2a–2c) demonstrate that these interpreted ChRM directions were acquired during or after local folding near Gamba County but before the regional folding within the Gamba and Tukson areas.

Considering the fast northward plate motion of Tibetan Himalaya during deposition of these rocks, one may question whether it is even meaningful to apply fold tests to either Member I or Members II–IV from a single section because differences in inclination are expected among these members. Given a maximum northward drift velocity of 180 mm/yr for India in the early Paleogene (placed in a paleomagnetic reference frame) [*van Hinsbergen et al.*, 2011a], the Tibetan Himalaya have moved ~540 km in ~3 Myr within the depositional time interval of Member I or Members II and III (Member IV has a depositional age of ~56–52 Ma, but the numbers of isolated ChRM directions from this member are limited, so we combined the samples from this member with those from Members II and III). This distance implies that a primary paleomagnetic inclination will record a drift of around ±5° from the inclination of the mean ChRM directions of Member I or Members II–IV at lower latitudes. This change in inclination is, however, within the statistical uncertainty of the mean inclination ($\Delta I = 5.6°$ for Member I; $\Delta I = 4.6°$ for Members II–IV). Therefore, the negative fold tests cannot be explained by plate motion.

The positive reversal tests (Figure 2d) from the Zongpu Formation are based on data from two short normal polarity zones determined from <10 samples [*Yi et al.*, 2011], which limits the statistical rigor of the test. Moreover, these normal polarity ChRM directions are very close to the present-day geomagnetic field (PDF) direction at the sampling locality in geographic coordinates (Figure 2d) and are suggestive of a recent overprint. If this interpretation is true, then this will make a correlation to GPTS meaningless. A few samples from the Jidula Formation below the Zongpu Formation also yielded similar normal polarity directions; they might record the same recent overprint as the specimens from Zongpu Formation, yielding normal polarity (Figure S2).

A higher paleolatitude determined from Members II to IV than that determined from Member I of the Zongpu carbonate rocks has also been used to argue for a primary remanence in these rocks. A careful inspection of the mean ChRM directions from Member I and Members II–IV indicates that the mean ChRM directions of Members II–IV share a common true mean direction (CTMD) with that of Member I with the classification of "A" in geographic coordinates. After tilt correction, however, the mean inclination of Members II–IV is ~10° steeper than that of Member I (Figures 2a and 2b). This difference in inclination is indeed similar to the difference in the mean bedding dip between Member I and Members II–IV strata (Figures 2e and 2f). Therefore, based on the above analyses, we argue that the apparent increase in inclination upsection is caused by applying a smaller bedding correction upsection to a uniform secondary remanent magnetization, which would coincidentally lead to an apparent northward paleolatitude shift. Therefore, the interpretation of a primary origin of the ChRMs isolated from the Zongpu carbonate rocks in previous studies is understandable, but inconclusive, and in the light of our new data, incorrect: the Zongpu carbonate rocks have been remagnetized.

Widespread remagnetization events are often interpreted to be linked to large-scale tectonic processes [e.g., *Elmore et al.*, 2012]. Orogenic fluids can be pumped by tectonically induced overpressures, or gravity, and migrate along aquifers or tectonic surfaces. Previous studies have shown that remagnetization of the Linzizong Group from the southern Lhasa terrane is probably assisted by such orogenic fluid flow

Figure 7. (a–e) Low-temperature demagnetization measurements for representative carbonate specimens. The specimens were magnetized isothermally at 300 K in a 2.5 t field, then measured in zero field while cooling to 20 K and rewarming (for 12ZP230 only) to room temperature. A Verwey transition is not observed. The Morin transition (~225 K in these samples) indicates the minor presence of nanohematite in some specimens. (f–j) Thermal demagnetization of low-temperature remanence shows progressive unblocking of the nanophase ferrimagnets, with no indication of the Verwey transition. FC remanence (for 12ZP230 only) was imprinted by cooling in a 2.5 t field from 300 K to 20 K; ZFC remanence was imparted isothermally at 20 K by application and removal of a 2.5 t field (after zero-field cooling from 300 K). Both remanences were measured while warming in zero field. (k–o) Particle-size distribution calculated for the ZFC curve in Figures 7f–7j according to *Worm and Jackson* [1999].

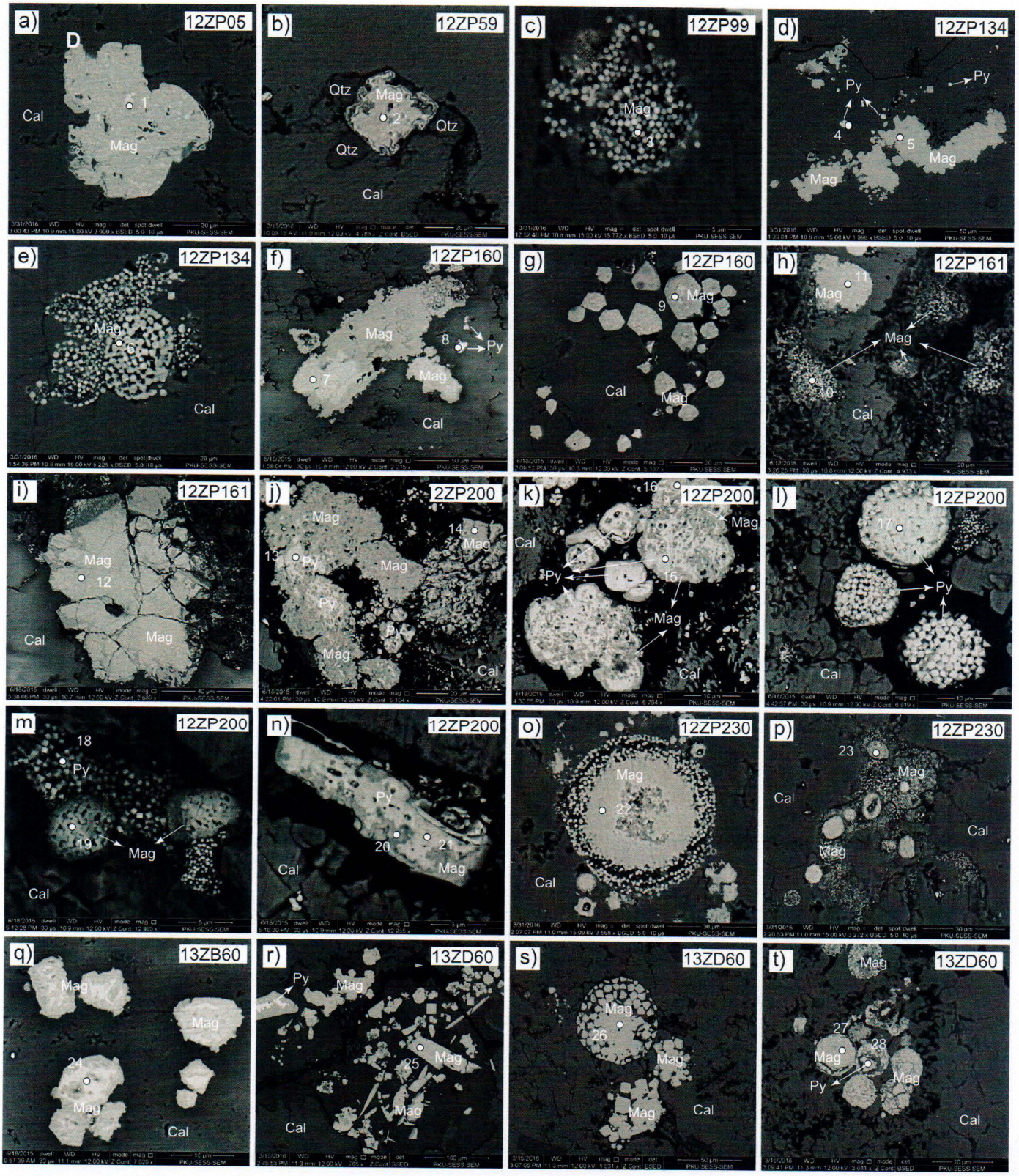

Figure 8. SEM backscattered electron images for selected specimens of the Zongpu carbonate rocks. Mag: magnetite, Cal: calcite, Qtz: quartz, Py: pyrite. The white dots with numbers indicate EDS analysis spots as shown in Figure S1.

[*Huang et al.*, 2015a, 2015b]. Circulation of oxidizing orogenic fluids may also account for the remagnetization of the carbonate rocks of the Zongpu Formation. Estimating the timing of remagnetization by plotting the mean ChRM direction of the Zongpu limestones on the declination and inclination plots of the GAPWaP curve of India [*Torsvik et al.*, 2012] at the coordinates of the studied section is not viable because this approach would assume that the Tibetan Himalaya were a contiguous part of the Indian continent and that crustal shortening within Tibetan Himalaya was negligible when remagnetization occurred. Both of these assumptions are controversial but critical for reconstructing the India-Asia collision. Fold tests on the data from the specimens from the four members of the Zongpu carbonate show that the best grouping is reached at ~25% untilting (Figure 2c). With this value of untilting, a mean inclination of ~36° can be estimated from these Zongpu specimens. This suggests that remagnetization occurred when the Zongpu carbonate rocks were located at a paleolatitude of ~20°N, immediately adjacent to the north of the southern margin of the Lhasa terrane at ~19°N during the early Paleogene [e.g., *van Hinsbergen et al.*, 2012; *Lippert et al.*, 2014; *Hu et al.*, 2016]. Therefore, it is reasonable to conclude that the remagnetization should have occurred during the widespread deformation and fluid circulation within the Tibetan Himalaya soon after onset of India-Asia collision.

6.2. Implications for Reconstructing the India-Asia Collision

When orogenic fluids remagnetized the Zongpu carbonate rocks in the Gamba area, they could also have remagnetized the Zongshan carbonate rocks at lower stratigraphic levels. The fold tests of the ChRMs from the Zongshan Formation in Gamba and Duina [*Patzelt et al.*, 1996] are inconclusive at best (Figure S3). Thorough rock magnetic and petrographic work required to verify this interpretation is beyond the scope of this paper, but in the light of the remagnetization of the Zongpu carbonate rocks documented here and the common remagnetization of other carbonate rocks across the Tibetan Himalaya [e.g., *Besse et al.*, 1984; *Liebke et al.*, 2013; *Huang et al.*, 2015c], the likelihood of remagnetization of the Zongshan carbonate rocks may be high. We now explore the tectonic implications from a perspective that the Zongshan carbonate rocks are also remagnetized. If this is the case, then there are no robust latitude estimates for the latest Cretaceous and early Paleogene positions of the Tibetan Himalaya. Thus, accurately dating the collision between India and Asia by using overlapping paleolatitudes of the Lhasa terrane and Tibetan Himalaya [e.g., *Dupont-Nivet et al.*, 2010; *van Hinsbergen et al.*, 2012; *Lippert et al.*, 2014; *Yang et al.*, 2015; *Hu et al.*, 2016], as widely applied, is unreliable. This realization can explain why the initiation of the collision constrained by paleomagnetism is significantly younger than the age determined from sedimentary records [e.g., *DeCelles et al.*, 2014; *Orme et al.*, 2014; *Hu et al.*, 2015, 2016; *Li et al.*, 2015].

Remagnetization of the Zongpu and Zongshan strata also implies that previous estimates of the late Cretaceous and Paleogene dimensions of Greater India, ranging from 1500 ± 480 km to 1900 ± 570 km [*Patzelt et al.*, 1996; *Yi et al.*, 2011], are no longer robust. Paleogene strata of the Sangdanlin section in southern Tibet record the earliest appearance of Asian-derived detritus deposited on top of the distal northern Indian margin at 59 ± 1 Ma [*Wang et al.*, 2011; *DeCelles et al.*, 2014; *Hu et al.*, 2015]. If we regard this age as the time of the initiation of the India-Asia collision [*Hu et al.*, 2015], then the size of Greater India must have been even larger than previously proposed: plate kinematic reconstructions of India and Asia [*van Hinsbergen et al.*, 2011a; *Huang et al.*, 2015d] require a size of Greater India with an N-S dimension of ~3800 km if we use the shortening reconstruction of Asia of *van Hinsbergen et al.* [2011b], or ~3500 km if we use the paleomagnetic data from Lhasa, suggesting a ~19°N Paleogene latitude [*Dupont-Nivet et al.*, 2010; *Lippert et al.*, 2014; *Hu et al.*, 2016]. A corollary is that the paleolatitudinal separation of the Tibetan Himalaya between the Early Cretaceous and the Paleogene was some 1500 km *more* than previously estimated [*van Hinsbergen et al.*, 2012]. This huge paleolatitudinal distance cannot be explained by counterclockwise rotation of India relative to Asia [*Huang et al.*, 2015d]. Rather, Greater India might have grown by extension to a much larger extent than previously assumed.

A total N-S dimension of 3500–3800 km of Greater Indian lithosphere is more than three times larger than estimates of crustal shortening within the Himalaya reconstructed from balanced cross sections [*DeCelles et al.*, 2002; *Long et al.*, 2011]. With the collision age assumed at 59 ± 1 Ma, the total India-Asia convergence from west to east has been ~3700–4600 km since collision began [*van Hinsbergen et al.*, 2011a]; the magnitude of lithospheric shortening within the upper plate over the same time interval has been on the order of 1500 km [e.g., *van Hinsbergen et al.*, 2011b]. A 59 ± 1 Ma collision age interpreted within a plate-kinematic

framework makes the discrepancy between convergence and crustal shortening even larger than that highlighted by *van Hinsbergen et al.* [2012]. Thus, although our study at first sight appears to obviate the Greater India Basin hypothesis of *van Hinsbergen et al.* [2012] by demonstrating that the latest Cretaceous to early Paleogene latitudes from the Tibetan Himalaya used to estimate the size of the Greater India are spurious, it instead indicates that, if the sedimentary record of initiation of the collision is accurate, then the requirement for Greater India extension is made ever greater.

7. Conclusions

Paleomagnetic data from carbonate rocks of the Zongpu Formation in the Gamba area were previously interpreted as providing the only "reliable" estimate for the Paleogene paleolatitude of the Tibetan Himalaya, an estimate that is used widely for the tectonic reconstructions of the India-Asia collision zone. Here we test the reliability of these data with a detailed sampling of the same section as the original paleomagnetic data. Our thorough reanalysis of the reported paleomagnetic directions, comprehensive rock magnetic tests, and petrographic investigations lead us to conclude that the Zongpu Formation carries a synfolding or postfolding remanent magnetization. Hematite occurs in some specimens, but the dominant ferromagnetic mineral is magnetite, >70% of which is superparamagnetic at room temperature and does not contribute to the remanence. The co-occurrence and petrographic relationships of pyrite and nanophase magnetite provide strong evidence that the carbonate rocks of the Zongpu Formation in the Gamba area were chemically remagnetized, with growth of authigenic magnetite from oxidizing orogenic fluids a likely remagnetization mechanism. Because the Zongpu Formation carries a secondary magnetite remanence, a reliable estimate for the Paleogene latitude of the Tibetan Himalaya remains unresolved and the paleomagnetically determined size of Greater India at the time of collision and the India-Asia collision age remain undetermined. An initiation of the collision age of 59 ± 1 Ma indicated by sedimentary records, kinematic reconstructions of the Indian and Eurasian plates, and the latitudes of southern Tibet at the time of collision requires a Greater India promontory with an N-S dimension of ~3500–3800 km in the early Paleocene. Compared to the Early Cretaceous paleolatitudes of the Tibetan Himalaya that show a Greater India extent of no more than a few hundred kilometers, the magnitude of late Cretaceous to Paleogene paleolatitudinal growth of India, necessarily by extension, might have been even larger than previously proposed.

Acknowledgments

Data to support this article are available in Tables S1–S3. This project was funded by the Netherlands Organization for Scientific Research (NWO) with a Rubicon grant (825.15.016) to W.H. The first author was also supported by the visiting research fellowship from the Institute for Rock Magnetism (IRM) at the University of Minnesota, which is funded by the Instruments and Facilities Program of NSF. We thank Peter A. Solheid at the IRM and Bo Zhang at Peking University for laboratory assistance. Xiumian Hu, Peter W. Reiners, Peter DeCelles, Barbara Carrapa, and Jay Quade are thanked for their inspiring discussions. Xiumian Hu is especially appreciated for sharing the samples collected by his group in the Gamba area. We are also grateful to R. Douglas Elmore, John W. Geissman, and Associated Editor Eric Ferré for their constructive comments.

References

Abrajevitch, A., and K. Kodama (2009), Biochemical vs. detrital mechanism of remanence acquisition in marine carbonates: A lesson from the K-T boundary interval, *Earth Planet. Sci. Lett.*, *286*(1), 269–277.

Appel, E., C. Crouzet, and E. Schill (2012), Pyrrhotite remagnetizations in the Himalaya: A review, *Geol. Soc. London Spec. Publ.*, *371*(1), 163–180.

Besse, J., V. Courtillot, J. P. Pozzi, M. Westphal, and Y. X. Zhou (1984), Paleomagnetic estimates of crustal shortening in the Himalayan thrusts and Zangbo suture, *Nature*, *311*, 621–626.

Chang, L., M. Winklhofer, A. P. Roberts, D. Heslop, F. Florindo, M. J. Dekkers, W. Krijgsman, K. Kodama, and Y. Yamamoto (2013), Low-temperature magnetic properties of pelagic carbonates: Oxidation of biogenic magnetite and identification of magnetosome chains, *J. Geophys. Res. Solid Earth*, *118*, 6049–6065, doi:10.1002/2013JB010381.

Day, R., M. Fuller, and V. Schmidt (1977), Hysteresis properties of titanomagnetites: Grain-size and compositional dependence, *Phys. Earth Planet. Int.*, *13*(4), 260–267.

DeCelles, P. G., D. M. Robinson, and G. Zandt (2002), Implications of shortening in the Himalayan fold-thrust belt for uplift of the Tibetan Plateau, *Tectonics*, *21*(6), 1062, doi:10.1029/2001TC001322.

DeCelles, P., P. Kapp, G. Gehrels, and L. Ding (2014), Paleocene-Eocene foreland basin evolution in the Himalaya of southern Tibet and Nepal: Implications for the age of initial India-Asia collision, *Tectonics*, *33*, 824–849, doi:10.1002/2014TC003522.

Dekkers, M. J. (2012), End-member modelling as an aid to diagnose remagnetization: A brief review, *Geol. Soc. London, Spec. Publ.*, *371*(1), 253–269.

Dunlop, D. J. (2002), Theory and application of the day plot (M_{rs}/M_s versus H_{cr}/H_c) 2. Application to data for rocks, sediments, and soils, *J. Geophys. Res.*, *107*(B3), 2057, doi:10.1029/2001JB000487.

Dunlop, D. J., and Ö. Ödemir (1997), *Rock Magnetism: Fundamentals and Frontiers*, pp. 573, Cambridge Univ. Press, Cambridge.

Dupont-Nivet, G., P. C. Lippert, D. J. J. van Hinsbergen, M. J. M. Meijers, and P. Kapp (2010), Palaeolatitude and age of the Indo-Asia collision: Palaeomagnetic constraints, *Geophys. J. Int.*, *182*(3), 1189–1198.

Elmore, R. D., A. R. Muxworthy, and M. Aldana (2012), Remagnetization and chemical alteration of sedimentary rocks, *Geol. Soc. London Spec. Publ.*, *371*(1), 1–21.

Fabian, K. (2003), Some additional parameters to estimate domain state from isothermal magnetization measurements, *Earth Planet. Sci. Lett.*, *213*(3), 337–345.

Guyodo, Y., A. Mostrom, R. Lee Penn, and S. K. Banerjee (2003), From nanodots to nanorods: Oriented aggregation and magnetic evolution of nanocrystalline goethite, *Geophys. Res. Lett.*, *30*(10), 1512, doi:10.1029/2003GL017021.

Hu, X., E. Garzanti, T. Moore, and I. Raffi (2015), Direct stratigraphic dating of India-Asia collision onset at the Selandian (middle Paleocene, 59 ± 1 Ma), *Geology*, *43*(10), 859–862.

Hu, X., E. Garzanti, J. Wang, W. Huang, W. An, and A. Webb (2016), The timing of India-Asia collision onset—Facts, theories, controversies, *Earth Sci. Rev.*, *160*, 264–299.

Huang, W., G. Dupont-Nivet, P. C. Lippert, D. J. van Hinsbergen, and E. Hallot (2013), Inclination shallowing in Eocene Linzizong sedimentary rocks from southern Tibet: Correction, possible causes and implications for reconstructing the India-Asia collision, *Geophys. J. Int.*, *194*(3), 1390–1411.

Huang, W., G. Dupont-Nivet, P. C. Lippert, D. J. Hinsbergen, M. J. Dekkers, R. Waldrip, M. Ganerød, X. Li, Z. Guo, and P. Kapp (2015a), What was the Paleogene latitude of the Lhasa terrane? A reassessment of the geochronology and paleomagnetism of Linzizong volcanic rocks (Linzhou Basin, Tibet), *Tectonics*, *34*, 594–622, doi:10.1002/2014TC003787.

Huang, W., et al. (2015b), Can a primary remanence be retrieved from partially remagnetized Eocence volcanic rocks in the Nanmulin Basin (southern Tibet) to date the India-Asia collision?, *J. Geophys. Res. Solid Earth*, *120*, doi:10.1002/2014JB011599.

Huang, W., et al. (2015c), Paleolatitudes of the Tibetan Himalaya from primary and secondary magnetizations of Jurassic to Lower Cretaceous sedimentary rocks, *Geochem. Geophys. Geosyst.*, *16*, 77–100, doi:10.1002/2014GC005624.

Huang, W., D. J. J. Van Hinsbergen, P. C. Lippert, Z. Guo, and G. Dupont-Nivet (2015d), Paleomagnetic tests of tectonic reconstructions of the India-Asia collision zone, *Geophys. Res. Lett.*, *42*, 2642–2649, doi:10.1002/2015GL063749.

Jackson, M. (1990), Diagenetic sources of stable remanence in remagnetized Paleozoic cratonic carbonates: A rock magnetic study, *J. Geophys. Res.*, *95*, 2753–2761, doi:10.1029/JB2095iB2703p02753.

Jackson, M., and N. L. Swanson-Hysell (2012), Rock magnetism of remagnetized carbonate rocks: Another look, *Geol. Soc. London Spec. Publ.*, *371*(1), 229–251.

Jackson, M., C. McCabe, M. M. Ballard, and R. Van der Voo (1988), Magnetite authigenesis and diagenetic paleotemperatures across the northern Appalachian basin, *Geology*, *16*(7), 592–595.

Klootwijk, C. T., and D. K. Bingham (1980), The extent of Greater India, III. Paleomagnetic data from the Tibetan sedimentary series, Thakkhola region, Nepal Himalaya, *Earth Planet. Sci. Lett.*, *51*(2), 381–405.

Lanci, L., and D. V. Kent (2006), Meteoric smoke fallout revealed by superparamagnetism in Greenland ice, *Geophys. Res. Lett.*, *33*, L13308, doi:10.11029/12006GL026480.

Li, J., X. Hu, E. Garzanti, W. An, and J. Wang (2015), Paleogene carbonate microfacies and sandstone provenance (Gamba area, South Tibet): Stratigraphic response to initial India-Asia continental collision, *J. Asian Earth Sci.*, *104*, 39–54.

Liebke, U., E. Appel, L. Ding, and Q. Zhang (2013), Age constraints on the India-Asia collision derived from secondary remanences of Tethyan Himalayan sediments from the Tingri area, *J. Asian Earth Sci.*, *62*, 329–340.

Lippert, P. C., D. J. J. van Hinsbergen, and G. Dupont-Nivet (2014), The Early Cretaceous to present latitude of the central Lhasa-plano (Tibet): A paleomagnetic synthesis with implications for Cenozoic tectonics, paleogeography and climate of Asia, in *Towards an Improved Understanding of Uplift Mechanisms and the Elevation History of the Tibetan Plateau*, *Geol. Soc. Am. Spec. Pap.*, vol. 507, edited by J. S. Nie, G. D. Hoke, and B. K. Horton, pp. 1–21, Geol. Soc. of Am., Boulder, Colo.

Long, S., N. McQuarrie, T. Tobgay, and D. Grujic (2011), Geometry and crustal shortening of the Himalayan fold-thrust belt, eastern and central Bhutan, *Bull. Geol. Soc. Am.*, *123*(7–8), 1427.

Ma, Y., T. Yang, W. Bian, J. Jin, S. Zhang, H. Wu, and H. Li (2016), Early Cretaceous paleomagnetic and geochronologic results from the Tethyan Himalaya: Insights into the Neotethyan paleogeography and the India-Asia collision, *Sci. Rep.*, *6*, 21605.

McFadden, P. L., and F. J. Lowes (1981), The discrimination of mean directions drawn from Fisher distributions, *Geophys. J. R. Astrol. Soc.*, *67*, 19–33.

McFadden, P. L., and M. W. McElhinny (1990), Classification of the reversals test in palaeomagnetism, *Geophys. J. Int.*, *103*, 725–729.

Najman, Y., E. Appel, M. Boudagher-Fadel, P. Bown, A. Carter, E. Garzanti, L. Godin, J. Han, U. Liebke, and G. Oliver (2010), Timing of India-Asia collision: Geological, biostratigraphic, and palaeomagnetic constraints, *J. Geophys. Res.*, *115*, B12416, doi:10.11029/12010JB007673.

Néel, L. (1949), Théorie du traînage magnétique des ferromagnétiques en grains fins avec applications aux terres cuites, *Ann. Geophys.*, *5*(2), 99–136.

Orme, D. A., B. Carrapa, and P. Kapp (2014), Sedimentology, provenance and geochronology of the upper Cretaceous-lower Eocene western Xigaze forearc basin, southern Tibet, *Basin Res.*, *27*, 387–411, doi:10.1111/bre.12080.

Özdemir, Ö., and D. J. Dunlop (2010), Hallmarks of maghemitization in low-temperature remanence cycling of partially oxidized magnetite nanoparticles, *J. Geophys. Res.*, *115*, B02101, doi:10.01029/02009JB006756.

Özdemir, Ö., D. J. Dunlop, and T. S. Berquo (2008), Morin transition in hematite: Size dependence and thermal hysteresis, *Geochem. Geophys. Geosyst.*, *9*, Q10Z01, doi:10.1029/2008GC002110.

Patzelt, A., H. Li, J. Wang, and E. Appel (1996), Palaeomagnetism of Cretaceous to Tertiary sediments from southern Tibet: Evidence for the extent of the northern margin of India prior to the collision with Eurasia, *Tectonophysics*, *259*, 259–284.

Roberts, A. P., Y. Cui, and K. L. Verosub (1995), Wasp-waisted hysteresis loops: Mineral magnetic characteristics and discrimination of components in mixed magnetic systems, *J. Geophys. Res.*, *100*, 17,909–17,924, doi:10.11029/17995JB00672.

Smirnov, A. V., and J. A. Tarduno (2001), Estimating superparamagnetism in marine sediments with the time dependency of coercivity of remanence, *J. Geophys. Res.*, *106*, 16,135–16,143, doi:10.11029/12001JB000152.

Sparks, N., S. Mann, D. Bazylinski, D. Lovley, H. Jannasch, and R. B. Frankel (1990), Structure and morphology of magnetite anaerobically-produced by a marine magnetotactic bacterium and a dissimilatory iron-reducing bacterium, *Earth Planet. Sci. Lett.*, *98*(1), 14–22.

Suk, D., D. Peacor, and R. Van der Voo (1990), Replacement of pyrite framboids by magnetite in limestone and implications for palaeomagnetism, *Nature*, *345*(6276), 611–613.

Tauxe, L., and G. Watson (1994), The fold test: An eigen analysis approach, *Earth Planet. Sci. Lett.*, *122*(3), 331–341.

Torsvik, T. H., R. Van der Voo, U. Preeden, C. Mac Niocaill, B. Steinberger, P. V. Doubrovine, D. J. J. van Hinsbergen, M. Domeier, C. Gaina, and E. Tohver (2012), Phanerozoic polar wander, palaeogeography and dynamics, *Earth Sci. Rev.*, *114*(3), 325–368.

van Hinsbergen, D. J., B. Steinberger, P. V. Doubrovine, and R. Gassmöller (2011a), Acceleration and deceleration of India-Asia convergence since the Cretaceous: Roles of mantle plumes and continental collision, *J. Geophys. Res.*, *116*, B06101, doi:10.01029/02010JB008051.

van Hinsbergen, D. J. J., P. Kapp, G. Dupont-Nivet, P. C. Lippert, P. G. Decelles, and T. H. Torsvik (2011b), Restoration of Cenozoic deformation in Asia and the size of Greater India, *Tectonics*, *30*, TC5003, doi:10.1029/2011TC002908.

van Hinsbergen, D. J. J., P. C. Lippert, G. Dupont-Nivet, N. McQuarrie, P. V. Doubrovine, W. Spakman, and T. H. Torsvik (2012), Greater India Basin hypothesis and a two-stage Cenozoic collision between India and Asia, *Proc. Natl. Acad. Sci. U.S.A.*, *109*(20), 7659–7664.

Wang, J., X. Hu, L. Jansa, and Z. Huang (2011), Provenance of the Upper Cretaceous-Eocene deep-water sandstones in Sangdanlin, southern Tibet: Constraints on the timing of initial India-Asia collision, *J. Geol.*, *119*(3), 293–309.

Worm, H. U., and M. Jackson (1999), The superparamagnetism of Yucca Mountain tuff, *J. Geophys. Res.*, *104*, 25,415–25,425, doi:10.21029/21999JB900285.

Yang, T., Y. Ma, W. Bian, J. Jin, S. Zhang, H. Wu, H. Li, Z. Yang, and J. Ding (2015), Paleomagnetic results from the Early Cretaceous Lakang Formation lavas: Constraints on the paleolatitude of the Tethyan Himalaya and the India-Asia collision, *Earth Planet. Sci. Lett.*, *428*, 120–133.

Yi, Z., B. Huang, J. Chen, L. Chen, and H. Wang (2011), Paleomagnetism of early Paleogene marine sediments in southern Tibet, China: Implications to onset of the India-Asia collision and size of Greater India, *Earth Planet. Sci. Lett.*, *309*(1), 153–165.

Zegers, T., M. Dekkers, and S. Bailly (2003), Late Carboniferous to Permian remagnetization of Devonian limestones in the Ardennes: Role of temperature, fluids, and deformation, *J. Geophys. Res.*, *108*(B7), 2357, doi:10.1029/2002JB002213.